Precision Measurement of Relativistic and QED Effects in Heliumlike Beryllium

T. J. Scholl, R. Cameron, S. D. Rosner, L. Zhang, and R. A. Holt
Physics Department, University of Western Ontario, London, Ontario, Canada N6A 3K7

Craig J. Sansonetti and J. D. Gillaspy
National Institute of Standards and Technology, Gaithersburg, Maryland 20899
(Received 25 May 1993)

We have used fast-ion-beam laser spectroscopy to measure the $1s2s\,^3S$-$1s2p\,^3P^o$ intervals in Be III to an absolute accuracy of 1 part in 10^8. Our results are (in cm^{-1}): $\sigma(1s2s\,^3S_1$-$1s2p\,^3P_0^o) = 26\,864.6120(4)$, $\sigma(1s2s\,^3S_1$-$1s2p\,^3P_1^o) = 26\,853.0534(3)$, $\sigma(1s2s\,^3S_1$-$1s2p\,^3P_2^o) = 26\,867.9484(3)$. These results are an improvement over previous measurements by nearly 3 orders of magnitude and show evidence of uncalculated $O(\alpha^4 Z^4)$ relativistic corrections. Once those terms are computed, our measurement will allow QED calculations in two-electron atoms to be tested at the 100 ppm level.

PACS numbers: 32.30.Jc

The calculation of relativistic and QED effects in one-electron atoms is based upon a well-understood theoretical framework in which perturbation theory is used to add QED effects to the Dirac equation. For the next most fundamental atomic system, two-electron atoms, the theoretical framework is not solidly established. The fully covariant Bethe-Salpeter equation has not led to a practical calculational method. Different approximation techniques have evolved for the low-Z and high-Z regions, but these make use of two-component partial Hamiltonians which are not covariant and whose extension to higher orders of perturbation theory poses difficulties.

At low Z, the best approach appears to be to solve the nonrelativistic Schrödinger equation variationally in a Hylleraas-type basis so as to include the strong electron-correlation effects accurately [1]. Relativistic and QED corrections are added as perturbations. The QED effects are of great interest because they include specifically two-electron diagrams for the electron-electron interaction and electron self-energy corrections which are absent in hydrogenic ions. The most accurate low-Z calculations are those by Drake, who has developed an improved basis [2] which yields nonrelativistic energy eigenvalues accurate to a few parts in 10^{15}. The accuracy of the total energies was estimated [3] as $\pm 1.2(Z/10)^4\ \mathrm{cm}^{-1}$, limited by uncalculated $O(\alpha^4 Z^4)$ relativistic corrections.

At high Z, one can begin with independent electrons obeying the Dirac equation and add both the static Coulomb repulsion and relativistic corrections by means of expansions in powers of Z^{-1} and αZ [4]. The multiconfiguration Dirac-Fock method [5,6] and Padé extrapolation [7] have also been used. Drake [3] has provided a unified set of results for $Z \leq 100$ in which variational calculations for low Z are smoothly joined to high-Z expansions. Johnson and Sapirstein [8] applied many-body perturbation theory for $10 \leq Z \leq 36$, and Chen, Cheng, and Johnson [9] carried out relativistic configuration interaction calculations for $5 \leq Z \leq 100$. These include most of the important $O(\alpha^4 Z^4)$ relativistic corrections, which they estimate as $-2.6(Z/10)^4$ for the $1s2s\,^3S_1$-$1s2p\,^3P_0^o$ wave number.

High-precision measurements on two-electron atoms have been carried out only on He I [10,11], Li II [12], and B IV [13]. Berry, Dunford, and Livingston [14] recently reviewed all the data for the helium isoelectronic sequence and concluded that the experimental values for the $1s2s\,^3S_1$-$1s2p\,^3P_0^o$ wave numbers are systematically lower than Drake's theoretical values by $\sim 2.3(Z/10)^4$ cm^{-1}.

In the present work, we report a fast-ion-beam laser-fluorescence measurement of the $1s2s\,^3S_1$-$1s2p\,^3P_{0,1,2}^o$ intervals in Be III to an absolute accuracy of 1 part in 10^8. The apparatus was an improved version of one which has been described in detail previously [15]. Be^{2+} ions were produced in a dc discharge (400 V, 50 mA) in a modified Danfysik 911A ion source using Be metal. The ions were extracted at chosen voltages between 7.5 and 10 kV, electrostatically focused, and mass selected with a Wien filter. The ions were then electrostatically deflected to make them collinear and overlapped with the laser beam, and refocused by a second einzel lens. Typical ion current was 15 nA. Collinear geometry narrowed the Doppler-limited linewidth by kinematic compression [16] to 850 MHz, corresponding to an energy spread of 4.3 eV per charge.

The 372 nm light used for excitation of the $2\,^3S$-$2\,^3P^o$ transitions was generated by intracavity frequency doubling in a cw Ti-sapphire ring laser. Typical uv power output was 45 mW, continuously tunable over 30 GHz in the fundamental frequency (60 GHz in the uv). The Doppler-shifted laser frequency was in resonance with the atomic transition only in a postacceleration region to which a 60 V potential was applied. Fluorescence from the $2\,^3P_J^o$ states is almost entirely back to the metastable $2\,^3S_1$ state and the small Doppler shift of $\sim 53\ \mathrm{cm}^{-1}$ did not permit blocking of scattered light, the major source of background. The light collection system consisted of a spherical retroreflection mirror, an f/0.75 lens, a field stop, and a second lens to focus light on a photomultiplier. Laser-induced fluorescence from a region 1 cm long by 2 mm high was imaged on the field stop aperture, providing improved scattered light rejection. The

0031-9007/93/71(14)/2188(4)$06.00

signal-to-background ratio was ~1:6. Doppler modulation with a 1-kHz, 10-V peak-to-peak ac voltage added to the postacceleration electrode was used so that a first derivative detection scheme could be employed. This detection scheme eliminated the sloping background and produced a steep zero crossing from which the line center was readily determined.

The overlap of the two beams within the viewing region of the optical system was critical for best signal-to-noise ratio. This geometry was defined by two small apertures which could be manipulated from outside the vacuum. After each alignment, these apertures were rotated out of the beams to reduce scattered light. The pointing of the laser was monitored by registering the laser beam on a second set of apertures, separated by 6.2 m, external to the vacuum. These guaranteed that the laser beam could be reversed with an accuracy of 1.6×10^{-4} rad, corresponding to an uncertainty in the ion-rest-frame wave number of 3.4×10^{-7} cm^{-1}.

As the laser was scanned by a computer, the fluorescence signals from the lock-in detector were recorded simultaneously with the laser power, the ion beam current, the transmission of the fundamental frequency through a heated I_2 absorption cell, and the transmission fringes from a low-finesse sealed, temperature-stabilized 1-GHz free-spectral-range (FSR) Fabry-Pérot etalon. Figure 1 shows typical fluorescence spectra for all three $2\,^3S_1$-$2\,^3P_J^o$ transitions. Each fine-structure (fs) component is split into 3 to 8 hyperfine (hf) components in the isotope ^{9}Be, with nuclear spin $I = \frac{3}{2}$. As can be seen, we have achieved complete resolution of the hyperfine structure (hfs).

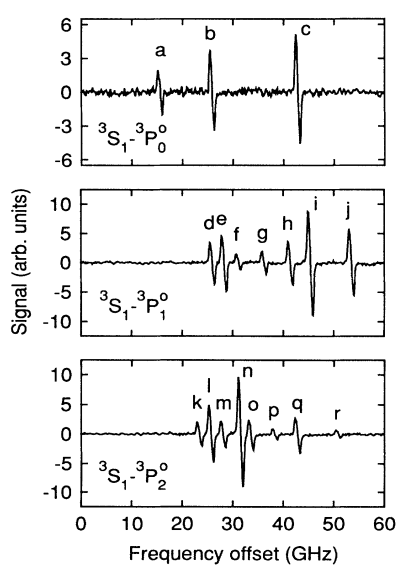

FIG. 1. Laser-induced fluorescence spectra for the fine-structure components of the $1s2s\,^3S$-$1s2p\,^3P^o$ transition in Be III. Lower-case letters label the hyperfine components; they are defined in Table II.

To minimize the effect of drift of the ion energy, a series of four measurements was made at a nominally fixed energy: one with the laser beam parallel to the ion velocity, followed by two antiparallel measurements, followed by a final parallel measurement. Since the Doppler profile reverses exactly with propagation direction, the absolute rest-frame wave numbers can be calculated precisely from the geometric mean of the corresponding red and blue Doppler-shifted wave numbers, if the ion energy is constant. The variation of the ion energy can be measured from shifts in the measured laboratory wave numbers. This analysis of all data yielded an rms scatter of 0.7 V, which implies an uncertainty of 1.62×10^{-3} cm^{-1} in the geometric mean. Three different accelerating voltages were used so as to make use of numerous calibration lines and to test for unsuspected voltage-dependent systematic errors. Each measurement was repeated on different days over several weeks, for a total of 36 spectra.

The fluorescence signal was normalized to the laser power and ion beam current and then least squares fit to the derivative of a Gaussian function to find each line center. The transmission peaks of the etalon signal were fit to an Airy function and then the centers of these were fit to a third-degree polynomial in channel number to establish a linear frequency scale. The I_2 spectrum is tabulated in several atlases; however, the accuracy in the infrared is only 5×10^{-3} cm^{-1} [17]. Hence, we used the I_2 absorption features merely as a set of markers for interpolation between 13 U lines which provided the absolute wave number calibration. The U lines were observed by optogalvanic spectroscopy in a commercial U-Ne hollow cathode lamp. We recorded 49 overlapping spectra of I_2 and U lines in the two regions containing the red- and blue-Doppler-shifted Be III lines.

The 13 U lines used for wave number calibration were measured in a separate experiment with the NIST Fabry-Pérot wave meter [18] using a similar hollow cathode lamp, as previously discussed [19]. The profile of each line was recorded by a computer which scanned the frequency of a Ti:sapphire laser across the line, digitized and stored the optogalvanic signal, and operated the wave meter to calibrate the scan. The digitized profile was fitted with a Voigt function to determine the line center. Scans were recorded in pairs with increasing and decreasing laser frequency under otherwise identical conditions and averaged to eliminate possible shifts due to laser and electronic settling times. The uncertainty for the average of each pair was calculated as the quadrature sum of the uncertainty of the wave number calibration and the uncertainty of the line center as determined in the least-squares fit. The two or three pairs of scans for each line were combined in a weighted average to yield the wave numbers given in Table I. The uncertainty for each line represents 1 standard deviation and is the quadrature sum of the uncertainty of the weighted average and an estimated 2.2×10^{-6} cm^{-1} uncertainty due to phase dispersion in the coatings of the

TABLE I. Wave numbers for optogalvanic uranium lines.

U Atlas[a] (cm^{-1})	Measured wave number (cm^{-1})	Difference (cm^{-1})
13 397.1596	13 397.158 06(7)	−0.0015
13 397.4905	13 397.489 87(5)	−0.0006
13 398.0382	13 398.036 80(7)	−0.0014
13 400.8889	13 400.887 79(4)	−0.0011
13 404.8749	13 404.873 56(5)	−0.0013
13 407.8850	13 407.885 12(7)	0.0001
13 411.8516	13 411.852 55(6)	0.0009
13 411.9748	13 411.973 53(5)	−0.0013
13 450.9792	13 450.978 15(5)	−0.0010
13 454.7516	13 454.750 58(5)	−0.0010
13 461.3127	13 461.311 67(5)	−0.0010
13 463.3924	13 463.391 62(4)	−0.0008
13 465.3046	13 465.303 32(7)	−0.0013

[a]Ref. [20]. Absolute uncertainty of all lines is 0.003 cm^{-1}.

Fabry-Pérot interferometer. Our values for these lines typically differ by about -1×10^{-3} cm^{-1} from earlier measurements made by Fourier transform spectroscopy [20].

Next, an overall least-squares adjustment was made with three types of observation equations involving absolute U wave numbers, offsets between U lines and selected I_2 lines in relative units of the reference etalon's FSR, and intervals between I_2 lines, also in FSR units. The Be III absolute wave numbers were then determined by interpolation from the calibrated I_2 lines, and the rest-frame wave numbers were extracted; these are listed in Table II. The statistical uncertainty in a single Doppler-shifted wave number was estimated by combining in quadrature the uncertainty in finding the center of the Be III derivative line shape (typically 0.5×10^{-3} cm^{-1}), the uncertainty in determining the I_2 calibration lines from the adjustment to the U lines (typically 0.9×10^{-3} cm^{-1}, which must be doubled since we are measuring the fundamental), and the uncertainty due to ion-beam energy drift (1.62×10^{-3} cm^{-1}). This yields a statistical uncertainty of $\sim 1.7 \times 10^{-3}$ cm^{-1} for a single measurement of a geometrical mean. Finally, we add twice the $\sim 6 \times 10^{-5}$ cm^{-1} absolute calibration uncertainty of the U lines in quadrature with the statistical uncertainty in the mean of N measurements.

We then removed the effects of hfs, including off-diagonal matrix elements. The magnetic dipole hfs of the $2\,^3P_J^o$ levels has been accurately calculated by Ohtsuki and Hijikata [21]; at $Z = 3$ the agreement with a precision experiment is within 1 MHz. We calculated the $2\,^3S_1$ magnetic dipole hfs using the value of $\langle\delta(r_1)\rangle$ from Ref. [1] and the value $g_I = -0.784\,967$ [22]. Although an $I = \frac{3}{2}$ nucleus can have electric quadrupole and magnetic octupole moments, the effect of these is negligible here. We used the measured values $\langle r^{-3}\rangle_{2p} = 1.0(2)$ a.u. [23] and $Q = +0.05$ b [22] to compute the electric quadrupole hfs using standard formulas [24], obtaining $B(2\,^3P_2^o) = 4.7$ MHz, $B(2\,^3P_1^o) = -2.4$ MHz, and $B(2\,^3P_0^o) = 0$. The wave number of each Doppler-free hf component was corrected for hfs, and the weighted mean for each of the three fs components was calculated. The residuals of all these hfs-free wave numbers, relative to their appropriate means, are presented as a histogram in Fig. 2. The 1.7×10^{-3} cm^{-1} standard deviation of this distribution is equal to the typical statistical uncertainty in a single measurement estimated above, confirming that the hfs subtraction contributes negligibly to our

TABLE II. Wave numbers σ of all hyperfine components of the $1s2s\,^3S_1$-$1s2p\,^3P_J^o$ transitions in Be III. Uncertainties represent 1 standard deviation. N = number of measurements.

Label[a]	J	$F(1s2s\,^3S_1)$	$F'(1s2p\,^3P_J^o)$	N	σ (cm^{-1})
a	0	$\frac{1}{2}$	$\frac{3}{2}$	6	26 864.0469(8)
b	0	$\frac{3}{2}$	$\frac{3}{2}$	6	26 864.3917(8)
c	0	$\frac{5}{2}$	$\frac{3}{2}$	6	26 864.9655(8)
d	1	$\frac{1}{2}$	$\frac{3}{2}$	6	26 852.5764(7)
e	1	$\frac{3}{2}$	$\frac{5}{2}$	6	26 852.6554(7)
f	1	$\frac{1}{2}$	$\frac{1}{2}$	6	26 852.7514(8)
g	1	$\frac{3}{2}$	$\frac{3}{2}$	6	26 852.9215(7)
h	1	$\frac{3}{2}$	$\frac{1}{2}$	6	26 853.0967(7)
i	1	$\frac{5}{2}$	$\frac{5}{2}$	6	26 853.2303(7)
j	1	$\frac{5}{2}$	$\frac{3}{2}$	5	26 853.4950(8)
k	2	$\frac{1}{2}$	$\frac{3}{2}$	6	26 867.6967(7)
l	2	$\frac{3}{2}$	$\frac{5}{2}$	6	26 867.7757(7)
m	2	$\frac{1}{2}$	$\frac{1}{2}$	6	26 867.8559(7)
n	2	$\frac{5}{2}$	$\frac{7}{2}$	6	26 867.9731(7)
o	2	$\frac{3}{2}$	$\frac{3}{2}$	6	26 868.0419(7)
p	2	$\frac{3}{2}$	$\frac{1}{2}$	6	26 868.1998(8)
q	2	$\frac{5}{2}$	$\frac{5}{2}$	6	26 868.3499(7)
r	2	$\frac{5}{2}$	$\frac{3}{2}$	4	26 868.6156(11)

[a]Labels refer to Fig. 1.

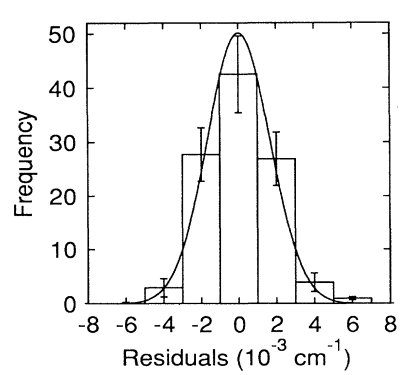

FIG. 2. Histogram of residuals for all measured transitions after correction for hyperfine structure and subtraction of the mean of each fine-structure component.

TABLE III. Wave numbers of the $1s2s\,^3S$-$1s2p\,^3P^o$ transitions in Be III (in cm^{-1}).

Transition	Experiment	Theory[a]	Expt−Theory
$2\,^3S_1$-$2\,^3P_0^o$	26 864.6120(4)	26 864.659	−0.047
$2\,^3S_1$-$2\,^3P_1^o$	26 853.0534(3)	26 853.060	−0.007
$2\,^3S_1$-$2\,^3P_2^o$	26 867.9484(3)	26 867.938	0.010

[a]Ref. [26].

error budget.

The weighted means of the three hf-free fs components (Table III) are in agreement with the measurements of Löfstrand [25] but are more precise by nearly 3 orders of magnitude. Also in Table III are new calculations by Drake [26], which use his high-precision variational wave functions and add relativistic reduced mass, relativistic recoil, and second-order mass polarization corrections not included in Ref. [3]. The major sources of uncertainty in the theory are those due to the still uncalculated $O(\alpha^4 Z^4)$ terms, originally estimated as $\pm 31 \times 10^{-3}$ cm^{-1} [3], and the uncertainty in the QED contributions, estimated as the size of the next uncalculated term in the Z^{-1} expansion of the two-electron Bethe logarithm: $\pm 14 \times 10^{-3}$ cm^{-1} and $\pm 5 \times 10^{-3}$ cm^{-1} for the $2\,^3S$ and $2\,^3P$ levels, respectively [26]. Using this QED uncertainty, our experiment can be viewed as measuring the $O(\alpha^4 Z^4)$ contribution to the $2\,^3S_1$-$2\,^3P_0$ interval to be $-47(15) \times 10^{-3}$ cm^{-1}. For comparison, the empirical fit of Berry *et al.* [14] yields -59×10^{-3} cm^{-1}, and the relativistic configuration interaction calculation of Chen *et al.* [9], whose validity is for higher Z, predicts -76×10^{-3} cm^{-1}. The QED contribution to these intervals is about 4.2 cm^{-1} [3]. Thus, once the relativistic terms are computed, our absolute accuracy of 1 part in 10^8 implies that we will be able to test QED calculations in two-electron atoms at the 100 parts per 10^6 level.

We thank the Natural Sciences and Engineering Research Council of Canada and the Academic Development Fund of the University of Western Ontario for financial support. We also thank G. W. F. Drake for allowing us to include his results in advance of publication.

[1] Y. Accad, C. L. Pekeris, and B. Schiff, Phys. Rev. A **4**, 516 (1971).
[2] G. W. F. Drake and A. J. Makowski, J. Opt. Soc. Am. B **5**, 2207 (1988).
[3] G. W. F. Drake, Can. J. Phys. **66**, 586 (1988).
[4] H. T. Doyle, Adv. At. Mol. Phys. **5**, 337 (1969); L. A. Vainshtein and U. I. Safronova, Phys. Scr. **31**, 519 (1985).
[5] J. Hata and I. P. Grant, J. Phys. B **16**, 523 (1983).
[6] P. Indelicato, Nucl. Instrum. Methods Phys. Res., Sect. B **31**, 14 (1988).
[7] R. DeSerio, H. G. Berry, R. L. Brooks, J. Hardis, A. E. Livingston, and S. J. Hinterlong, Phys. Rev. A **24**, 1872 (1981).
[8] W. R. Johnson and J. Sapirstein, Phys. Rev. A **46**, R2197 (1992).
[9] M. H. Chen, K. T. Cheng, and W. R. Johnson, Phys. Rev. A **47**, 3692 (1993).
[10] P. Zhao, J. R. Lawall, A. W. Kam, M. D. Lindsay, and F. M. Pipkin, Phys. Rev. Lett. **63**, 1593 (1989).
[11] C. J. Sansonetti, J. D. Gillaspy, and C. L. Cromer, Phys. Rev. Lett. **65**, 2359 (1990).
[12] E. Riis, H. G. Berry, O. Poulsen, S. A. Lee, and S. Y. Tang, Phys. Rev. A **33**, 3023 (1986).
[13] T. P. Dineen, N. Berrah-Mansour, H. G. Berry, L. Young, and R. C. Pardo, Phys. Rev. Lett. **66**, 2859 (1991).
[14] H. G. Berry, R. W. Dunford, and A. E. Livingston, Phys. Rev. A **47**, 698 (1993).
[15] T. J. Scholl, R. A. Holt, and S. D. Rosner, Phys. Rev. A **39**, 1163 (1989).
[16] S. L. Kaufman, Opt. Commun. **17**, 309 (1976).
[17] S. Gerstenkorn, J. Vergès, and J. Chevillard, *Atlas du spectre d'absorption de la molécule d'iode*, 11 000 cm^{-1}–14 000 cm^{-1} (Laboratoire Aimé Cotton, Orsay, 1982).
[18] C. J. Sansonetti, in *Advances in Laser Science IV*, Proceedings of the Fourth International Laser Science (ILS) Conference, Atlanta, GA, edited by James L. Gole *et al.*, AIP Conf. Proc. No. 191 (AIP, New York, 1989), p. 548.
[19] C. J. Sansonetti and K.-H. Weber, J. Opt. Soc. Am. B **1**, 361 (1984).
[20] B. A. Palmer, R. A. Keller, and R. Engleman, Jr., *An Atlas of Uranium Emission Intensities in a Hollow Cathode Discharge*, LASL Report No. LA-8261-MS (Los Alamos Scientific Laboratory, Los Alamos, NM, 1980).
[21] K. Ohtsuki and K. Hijikata, J. Phys. Soc. Jpn. **57**, 4150 (1988).
[22] G. H. Fuller, J. Phys. Chem. Ref. Data **5**, 835 (1976).
[23] O. Poulsen and J. L. Subtil, J. Phys. B **7**, 31 (1974).
[24] A. Lurio, M. Mandel, and R. Novick, Phys. Rev. **126**, 1758 (1962).
[25] B. Löfstrand, Phys. Scr. **8**, 57 (1973).
[26] G. W. F. Drake (private communication).